of the amplitude pattern effect into the spectral patterning in the SOA.[7] Suppression of the spectral broadening with a low-finesse Fabry–Perot in-line filter, effects of the SOA figure of merit,[6] and influences of the SOA current map along the line on the system performance are also considered.

1. J.J.E. Ried, P.I. Kuindersma, G.P.J.M. Cuijpers, G.N. van den Hoven, S. Walczyk, B. Teichmann, C. Dorschky, R. Seitz, C. Schulien, L. Cucala, H. Gruhl, R. Leppla, A. Mattheus, in *Technical Digest of ECOC, 1997*, Vol. 1, pp. 83–86.
2. M. Settembre, M. Tamburrini, F. Matera, H. Haunstein, B. Teichmann, I. Gabitov, E. Laedke, K. Spatschek, S.K. Turitsyn, J.J.E. Ried, in *Technical Digest of ECOC, 1997*, Vol. 1, pp. 75–78.
3. A. Shipulin, G. Onishchukov, P. Riedel, D. Michaelis, U. Peshel, F. Lederer, Electron. Lett. **33,** 507–508 (1997).
4. M. Settembre, F. Matera, V. Hägele, I. Gabitov, A. Mattheus, S. Turitsyn, J. Lightwave Technol. **15,** 962–967 (1997).
5. P.I. Kuindersma, G.P.J.M. Cuijpers, J.G.L. Lennen, J.J.E. Ried, L.F. Tiemeijer, H. de Waardt, A.J. Boot, in *Technical Digest of ECOC, 1996*, Vol. 2, paper TuD.2.1, pp. 165–168.
6. A. Shipulin, G. Onishchukov, P. Riedel, D. Michaelis, U. Peschel, F. Lederer, in *Optical Fiber Communication Conference*, Vol. 2 of OSA 1998 Technical Digest Series (Optical Society of America, Washington, DC, 1998), paper ThO6.
7. P.I. Kuindersma, G.P.J.M. Cuijpers, J.J.E. Ried, G.N. van den Hoven, S. Walczyk, in *Technical Digest of ECOC, 1997*, Vol. 1, pp. 79–82.

CThU4 **3:15 pm**

Experimental demonstration of spectrally encoded optical CDMA systems using Mach–Zehnder encoder chains

Cedric F. Lam, Rutger Vrijen, Dennis T.K. Tong, Ming C. Wu, Eli Yablonovitch, *Electrical Engineering Department, UCLA, Los Angeles, California 90095-1594*

Recently, there has been tremendous interest in applying spread spectrum and code-division multiple access (CDMA) techniques in optical fiber communication systems. Contrary to radio CDMA systems,[1] which employs electric-field encoding and correlation to achieve orthogonality, most of the optical communication systems use intensity modulation and direct detection. To achieve true orthogonality in optical CDMA systems, the balanced detection scheme and spectral intensity coding need to be used.[2]

Figure 1 shows the block diagram of the bipolar spectrally encoded CDMA system. The transmitter consists of a pair of broadband optical sources connected in a balanced fashion. The input data differentially modulate the intensity of the two balanced sources. The spectrum from the broadband sources passes through a dual-channel complementary spectral intensity encoder. When a 0 bit is sent, the transmitter encodes the direct spectrum for transmission. When a 1 bit is sent, the complementary spectrum is encoded. The intensity encoded spectra are broadcast to the receivers using a star coupler. The balanced receiver uses the same spectral encoder to recover the data. It can be seen from Fig. 1 that the receiver computes the difference signal between the direct spectrum and its complementary. For matched transmitter, the balanced receiver will detect either a positive or a negative output depending on whether 0 or 1 is transmitted. The spectra from unmatched transmitters will split equally at the two output ports of the receiver filter and will be canceled at the balanced output, hence achieving true orthogonality.

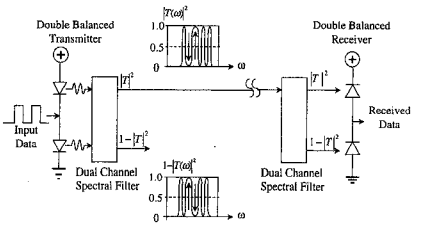

CThU4 Fig. 1. Block diagram of spectrally encoded fiber-optic CDMA system.

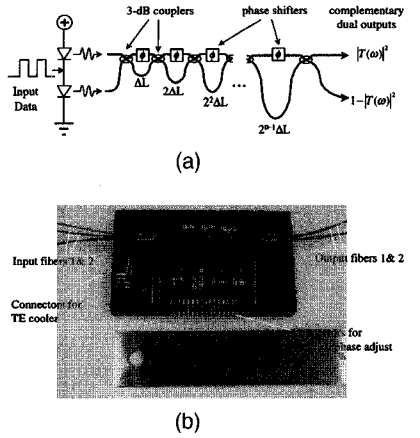

CThU4 Fig. 2. (a) Schematic diagram of the Mach–Zehnder interferometer encoder chain. (b) Fabricated MZI encoder chain on silica planar waveguide.

A multistage Mach–Zehnder interferometer (MZI) chain is proposed as the dual-channel spectral filter. The outputs of an MZI are automatically complementary. In addition, when the input source is switched from one input port to the other, the two complementary spectra at the MZI output ports will be reversed. Figure 2(a) shows the schematic diagram of an encoder and Fig. 2(b) shows a seven-stage MZI encoder chain fabricated on a planar silica waveguide. A thin-film heater is incorporated in each stage of the MZI encoder to introduce an optical phase shift in the MZI arms. Different codes are produced by properly setting the phase shifts at different stages. The chip size is 45.5 × 64 mm. Each thin-film heater is capable of shifting the optical phase by at least 2π rad.

An optical CDMA test bed has been built at UCLA to demonstrate the system principle. In the testbed setup, an erbium-doped fiber amplifier (EDFA) pumped into superluminescent mode and a 2×2 electro-optic switch are used to simulate the balanced transmitter. A preliminary experiment at 100 M bps was performed using the test bed. By matching the transmitter and receiver code settings, a 2^7-1 pseudorandom test data sequence is recovered at the receiver. We have also seen the rejection when the transmitter and receiver codes are unmatched. A bit error rate of 10^{-7} was achieved for this preliminary experiment. Figure 3 shows the eye diagram obtained from the experiment.

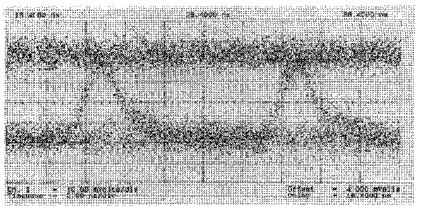

CThU4 Fig. 3. Eye diagram obtained from a 100 M bps 2^7-1 pseudorandom test data sequence.

This work is supported by the U.S. Air Force/Office of Scientific Research under contract F49620-95-1-0534.

1. R.L. Peterson, R.E. Ziemer, D.E. Borth, *Introduction to Spread Spectrum Communications* (Prentice Hall, Englewood Cliffs, N.J., 1995).
2. M. Kvehrad, D. Zaccarin, J. Lightwave Technol. **13,** 534–545 (1995).

CThU5 **3:30 pm**

BER analysis of low-rate communications through a single electro-optic R2 nonlinear regenerator

Richard A. Barry, Muriel Medard,* *MIT Lincoln Laboratory, 244 Wood Street, C-249, Lexington, Massachusetts 02173; E-mail: ribarry@ll.mit.edu*

Recently, the benefits of electro-optic nonlinear untimed regeneration (R2) for bit-rate transparent lightwave OOK systems have been expounded.[1–3] Here, we compare R1 (linear amplification), R2, and R3 (optimal DEMOD/MOD) in the presence of average white Gaussian noise (AWGN). We provide an approximate analysis and explain the difficulties in obtaining an exact solution.

The analyzed system is shown in Fig. 1. A modulated OOK signal $s(t)$ is transmitted. After a loss L_1, the signal is detected, filtered, thresholded, and retransmitted as in Refs. 1–3. AWGN is present in the electrical domain. After another loss L_2, the signal is again detected and demodulated using a matched filter receiver. We consider one-shot communication so that jitter and induced spatial coherence (ISI) can be ignored. In this case, the analysis applies equally well to return to zero (RZ) and non-return to zero (NRZ). Reference 1 addresses jitter but not noise. Reference 3 is experimental and shows a benefit of R2. Reference 2 provides an analysis for an arbitrary num-

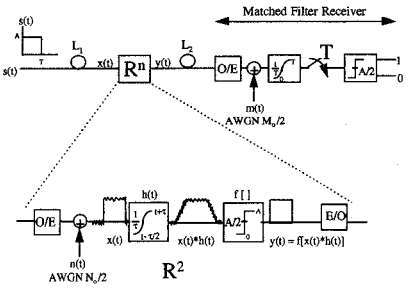

CThU5 Fig. 1. System configuration with R2 blowup.

ber of regenerators; however, we feel that the region in which this analysis is valid provides a misleading and unfair comparison among R1, R2, and R3.

For simplicity and tractability, R2 is modeled as a front-end filter $h(t)$ and a time-invariant thresholder $f[\,]$. The filter is modeled as a running integrator of width τ. Also shown is a 1 pulse of width T through R2. In the following, the losses L_1 and L_2 are normalized, without loss of generality, to 1.

An exact analysis of R2 requires the probability density function (pdf) $p_I(I)$ of

$$I = \frac{1}{T}\int_0^{\tau} f[s(t)*h(t) + n(t)*h(t)]dt$$

conditioned on a 1 or 0 being sent. We are unaware of a closed-form solution to $p_I(I)$. Reference 4 provides bounds on $p_I(I)$ for $T = \tau$. Reference 2 ignores the receiver filter (the integral in the above expression) and hence is applicable only for large receiver bandwidths (BWs) where the integrand can be modeled as constant for a bit time. In this case, I can be approximated as Bernoulli; however, this is an unfair comparison because the performances of R1, R2, and R3 systems can all be improved by reducing the receiver BW.

We limit our discussion to $b = T/\tau \gg 1$ so that $s(t) * h(t) \approx s(t)$. Note that because τ must accommodate the maximum supported bit rate (recall that the system is meant to be bit-rate transparent), our analysis applies to transmission of lower-rate signals.

For large b, we approximate $p_I(I)$ by sampling the integrand at the Nyquist rate and assume $n(t)$ is constant within a correlation time τ. This provides b statistically independent samples and thus, $p_I(I)$ is approximately binomial with mean $Q(E_b/bN_o)$ if 0 was sent and $A[1 - Q(E_b/bN_o)]$ if 1 was sent, where $E_b = A^2T/2$ is the average energy per bit. Simulations have indicated that the binomial is a more accurate approximation than a Gaussian.

Figure 2 shows the approximate bit error rate for various ratios of noise before and after the regenerator. Each plot shows the effect of $b = 5, 10, 20$ on R2 and the exact results for R1 and R3.

For $N_o \gg M_o$, e.g., regeneration near the egress, R2 performs worse than R1, as expected since (1) the cascade of the regenerator and the receiver can be modeled as a single receiver, (2) a matched filter receiver

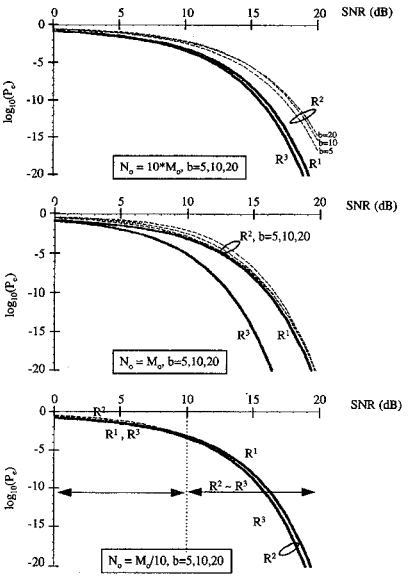

CThU5 Fig. 2. BER vs. SNR = $E_b/(N_o + M_o)$ for R1, R2 (b = 5, 10, 20), and R3.

is optimal, and (3) the cascade does not form a matched filter.

For $N_o \ll M_o$, e.g., regeneration near the ingress, R2 performs worse than R1 at small SNRs and better than R1 at high SNRs. The crossover SNR increases with b, and hence the required SNR into R2 (to perform at least as well as R1) increases with decreasing bit rates. However, for $N_o \ll M_o$, any reasonable regeneration device will have comparable performance.

For $N_o = M_o$, R2 performs uniformly worse than R1. Although this approximate analysis does not preclude the possibility of a crossover at high SNRs, it appears likely that no significant performance improvements can be achieved at SNRs of interest. Hence, R2 probably does not provide significant distance extension when used as a midspan repeater.

In summary, we find that R2 degrades noise sensitivity for low-rate signals unless the input SNR is high. Even in these cases, the improvement is small. Hence, R2 alone does not motivate electro-optic conversion in that an EDFA has better noise properties than an electro-optic R2. However, if the SNR is large and conversion to electronics is required, e.g., for wavelength conversion at the ingress of an all-optical network, R2 can provide small improvements.

MIT Lincoln Laboratory

1. P.E. Green, F.J. Janniello, R. Ramaswami, IEEE J. Select. Areas Commun. **14,** 962–967 (1996).
2. P. Ohlen, E. Berglin, IEEE Photonics Technol. Lett. **9,** 1011–1013 (1997).
3. K. Inoue, M. Jinno, IEEE Photonics Technol. Lett. **9,** 109–111 (1997).
4. J.E. Mazo, J. Salz, L.A. Shepp, Error rates on a data link with nonlinear regeneration, in *IEEE Transactions on Communications,* **COM-21** (1973).

CThV

2:30 pm–4:00 pm
Room 105

Solitons and Other Novel Photorefractive Effects

David D. Nolte, *Purdue University, Presider*

CThV1 2:30 pm

One-dimensional steady-state photorefractive spatial solitons in centrosymmetric paraelectric KLTN

Eugenio Del Re,* Bruno Crosignani,**
Mario Tamburrini, Mordechai Segev,†
Matthew Mitchell,† Eli Refaeli,‡
Aharon J. Agranat,‡ *Fondazione Ugo Bordoni, Via B Castiglione 59, Rome 00142 Italy*

Photorefractive spatial solitons have been the subject of intense study over the past few years. They have been predicted and observed in quasi-steady-state, steady state in photovoltaic materials, the steady-state screening configuration, and photorefractive semiconductors. More complicated phenomena have also been reported, giving rise to a wealth of intriguing observations, such as self-trapping of incoherent white-light beams and soliton-soliton interactions. All these have been observed in noncentrosymmetric materials, where soliton formation is brought about by a change in the refractive index due to the linear electro-optic response to an internal photoinduced space-charge field. Recently, spatial screening solitons of a different nature than should exist in photorefractive centrosymmetric materials have been predicted.[1] Here, we report the first observation of such solitons in paraelectric (centrosymmetric) KLTN and compare our experiments to the theoretical predictions.

Centrosymmetric screening solitons are generated by the index modulation produced by the quadratic electro-optic response to the photorefractive internal photoinduced field. The internal field has, in this case, the double role of both polarizing the ionic crystalline structure and distorting the standard electronic polarization. In centrosymmetric crystals, the change in refractive index is proportional to the square of the polarization $(1/n)_{ij} = g_{ijkl} P_k P_l$ and is therefore expressed in the typical screening configuration by $\Delta n = -(1/2) n_b^3 g_{\text{eff}} \varepsilon_0^2 (\varepsilon_r - 1)^2 E^2$, where E is the internal field, g_{eff} the effective quadratic electro-optic coefficient, and n_b the background refractive index, assuming that the dc polarization is in the linear regime, i.e., $P = \varepsilon_0(\varepsilon_r - 1)E$.

Our experiments are performed in KLTN,[2] which is specifically treated to have a first-order ferroelectric-paraelectric phase transition slightly below room temperature. Working at room temperature enables one to operate in a centrosymmetric phase close to the phase transition, thereby enhancing the electro-optic response,[2] making centrosymmetric soliton observation possible with moderate electric fields. In particular, since Δn scales with $(\varepsilon_r - 1)^2$, operation at temperatures slightly above the Curie temperature results in an increase in the quadratic electro-optic response.